Available online at www.sciencedirect.com
ScienceDirect
International Journal of Heat and Fluid Flow 28 (2007) 95–102
International Journal of HEAT AND FLUID FLOW
www.elsevier.com/locate/ijhff

Experimental investigation of transient boiling heat transfer in microchannels

M. Cortina Díaz, J. Schmidt *

Institute of Fluid Dynamics and Thermodynamics, Otto-von-Guericke University of Magdeburg, Universitätsplatz 2, D-39106 Magdeburg, Germany

Accepted 20 May 2006
Available online 1 September 2006

Abstract

This paper presents an experimental investigation of flow boiling heat transfer in a single $0.3 \times 12.7\ mm^2$ rectangular microchannel. Water and ethanol are employed as test fluids. The test section, which is made of the nickel alloy Inconel 600, is electrically heated. The examined parameter ranges are: mass fluxes between 50 and 500 kg/m^2s and heat fluxes up to 400 kW/m^2 at an outlet pressure of 0.1 MPa. Infrared thermography is employed to register the outer wall temperatures of the channel. This measurement method is especially appropriate for the analysis of the transient behavior of boiling in microchannels, which has been often reported in the literature. Infrared images of the test section are recorded at a frequency of 150 Hz using the half image mode. Data are collected over 25 s and the behavior of the obtained wall temperatures is analyzed. Local heat transfer coefficients are then calculated from the time averaged outer wall temperatures. Finally, the experimental values are compared with widely used correlations.

Keywords: Heat transfer; Flow boiling; Microchannels

1. Introduction

Flow boiling heat transfer in small channels is becoming increasingly important due to the high heat transfer rates and to their growing technical potential, for example in chemical process engineering. Although the number of investigations has increased rapidly in recent years, some aspects still remain unclear. For example, no generally accepted correlations are available for calculation of the heat transfer coefficients and pressure drop. Also, the lower limit of the hydraulic diameter, for which classical correlations for conventional channels remain applicable, is still to be identified. However, thanks to the support of high resolution visualizations, some light has been shed on the problem of boiling in small channels. Nucleate boiling seems to play an important role, either in formation of elongated bubbles, which develop into slugs and fill the entire channel, or bubbles which nucleate in the thin liquid film near the wall. An experimental study including high resolution visualizations was presented in Kandlikar and Balasubramanian (2004). Water flowing through six parallel minichannels, each 1054 μm wide and 197 μm deep, was investigated. Three gravitational orientations were compared under the same operating conditions. Bubbly flow, thin film nucleation, slug flow and churn flow were observed in all three orientations. Flow patterns were found to be time dependent. Decreasing trends in heat transfer coefficients with increasing quality were reported. These trends were in agreement with observations, where nucleating bubbles were detected at the wall during liquid flow and also in the liquid film near the wall in plug or annular flow. It was concluded that nucleate boiling was the dominant boiling mechanism. In Bao et al. (2000), flow boiling heat transfer of Freon R11 and HCFC123 in an electrically heated horizontal smooth copper tube with an inner diameter of 1.95 mm was studied. The parameter ranges were: heat

* Corresponding author. Tel.: +49 391671 8576; fax: +49 391671 2762.
E-mail address: juergen.schmidt@vst.uni-magdeburg.de (J. Schmidt).

0142-727X/$ - see front matter © 2006 Elsevier Inc. All rights reserved.
doi:10.1016/j.ijheatfluidflow.2006.05.008

Nomenclature

a	thermal diffusivity
Bo	boiling number, $Bo = q/mh_{fg}$,
c_{Fl}	specific heat capacity, J/kgK
Fo	Fourier number, $Fo = at/l_{ch}^2$,
h	channel height, m
h_{fg}	latent heat of vaporization, J/kg
K_1	non-dimensional group, (Kandlikar, 2004), $K_1 = (q/mh_{fg})^2\ \rho_L/\rho_V$
l_{ch}	characteristic length, m
m	mass flux, kg/m^2 s
p	pressure, Pa
q	heat flux, W/m^2
T	temperature, °C
t	time, s
w	channel width, m
x	vapor quality, –
z	axial position, m

Greek symbols

α	heat transfer coefficient, W/m^2 K
ρ	density, kg/m^3

Subscripts

B	saturation
Fl	fluid
IN	inlet
iw	inner wall
L	liquid
ow	outer wall
V	vapor

fluxes from 5 to 200 kW/m^2, mass fluxes between 50 and 1800 kg/m^2 s and system pressures from 200 to 500 kPa. The heat transfer coefficient was found to be independent of the mass flux and vapor quality, but it depended on both pressure and heat flux. Therefore, nucleate boiling was proposed as the dominant heat transfer mechanism. In Shuai et al. (2004), flow visualization during flow boiling of deionized water was carried out. Two test specimens were used: 2×4 mm^2 and 0.86×2 mm^2. Mass fluxes between 50 and 100 kg/m^2 s and heat fluxes from 10 to 180 kW/m^2 were examined. Flow patterns usually reported in the literature as bubbly flow, slug flow and annular flow were observed. Also, local dry out and large-amplitude pressure drop oscillations, as well as flow reversal, were reported.

Flow instabilities were also reported in Brutin et al. (2003), where *n*-pentane was used as the working fluid. Rectangular microchannels covered with polycarbonate plates of hydraulic diameter of 889 μm were employed. The presence of two-phase flow oscillations in flow boiling was observed. Steady and unsteady flow boiling, which depended on the operating conditions, were identified and stability criteria were obtained. Steady state was defined by low fluctuation amplitude and no characteristic oscillation frequency and unsteady state was identified by higher fluctuation amplitudes (>1 kPa) and a characteristic oscillation frequency. The following two-phase behavior was reported: liquid filled the channel, bubbles nucleated and coalesced to vapor slugs. These slugs generated overpressure, which reduced the upstream boiling flow rate. Expanding vapor pushed the inflow back to the entrance and the channel was finally filled with vapor. The vapor slug which occupied the entire channel was expelled, the channel was refilled with liquid and the cycle started again.

A recent study of the unsteady behavior of boiling in small channels can be found in Xu et al. (2005). The test section consisted of ten triangular microchannels with the hydraulic diameter of 155.4 μm. Acetone was used as the working fluid. The outer wall temperatures on the heating side of the silicon wafer were measured by an infrared camera. The front side of the silicon wafer was a pyrex glass cover for visualization using a high speed camera. Both measurement methods allow for the linking of the transient flow pattern observation and the determination of the heat transfer coefficient. The authors proposed the boiling number, Bo, as the key for establishing the relative dominance of boiling mechanisms, since it gives information on the evaporation momentum force relative to the inertia force. When different working fluids are considered, the use of the factor K_1 derived by Kandlikar (2004) was suggested. The boiling cycle was divided in three substages, viz. liquid refilling, bubble nucleation, growth and coalescence and transient liquid film evaporation stage. The heat transfer coefficient was found to increase with quality for low Bo numbers, be independent of mass flux and quality for medium Bo numbers and decrease with quality for high Bo numbers. In Lin et al. (2001), two-phase heat transfer to R141b in a 1 mm internal diameter vertical tube was investigated. The test section was electrically heated. Mass fluxes between 300 and 2000 kg/m^2 s and heat fluxes from 10 to 1150 kW/m^2 were examined. For low heat fluxes, the heat transfer coefficients increased first with quality, indicating the onset of subcooled nucleate boiling, decreased then at low qualities, where nucleate boiling dominated and increased finally at higher qualities, indicating convective boiling. It was also observed that, after a certain value of heat flux, the heat transfer coefficients decreased with quality. This decrease was attributed to the over-prediction of the heat transfer coefficient for high heat fluxes due to the linear approximation of the pressure drop in the data reduction. It was suggested that, a significant portion of the pressure drop would occur at the onset of boiling with the generation of confined bubbles, particularly at high heat fluxes. The pressure and saturation temperature may be somewhat lower in the low quality region of the tube

than predicted by a linear pressure drop. It was also observed that both wall temperature and fluid saturation temperature vary with time.

However, boiling in mini and microchannels seems to occur as a combination of both nucleate and convective boiling mechanisms. Some overviews of the progress made in the field of boiling in small channels can be found in Groll and Mertz (2003); Kandlikar (2002); Thome (2004). Reported discrepancies can be due to the use of different test conditions or measurement methods, as well as due to measurement accuracy. Therefore, further research is needed to develop reliable design tools, which will allow for the use of microchannels in industry.

The present study focuses on the experimental investigation of boiling heat transfer in a single rectangular microchannel. In contrast to many of the available experimental studies, where thermocouples were employed to measure the wall temperature, infrared thermography is employed here to scan the outer wall temperatures. Through these means, a continuous and contactless measurement of the wall temperature distribution is possible without time delay. The transient behavior of boiling will be analyzed for two test fluids, viz. water and ethanol. This transient analysis aims to contribute to a better understanding of boiling mechanisms in mini and microchannels, as well as to obtain reliable values of the heat transfer coefficients. The experimental heat transfer coefficients are presented and compared with predictions of available correlations.

2. Experimental setup

The experimental apparatus is shown in Fig. 1. The working fluid leaves the reservoir and flows through the gear pump, the heat exchanger and the mass flow meter into the test section. The desired mass flow is adjusted by the dosing pump and controlled by the mass flow meter, which operates according to the Coriolis principle. The heat exchanger provides the desired inlet temperature of the fluid. The test section is a rectangular channel made of the nickel alloy Inconel 600 and has the following dimensions: 0.3 mm height, 12.7 mm width and 200 mm length. The wall thickness is 0.3 mm. The fluid flows upwards, and the test section is electrically heated. Two

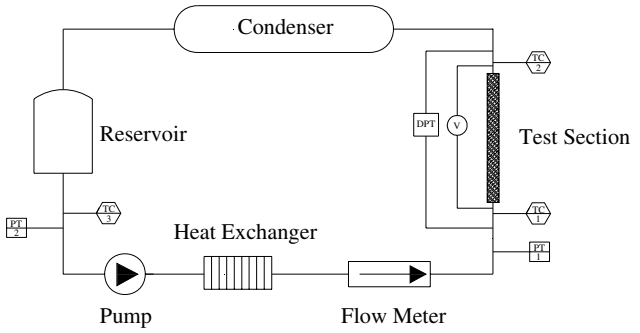

Fig. 1. Process diagram.

Table 1
Experimental accuracy of the measured values

Quantity	Accuracy/Parameter range
Inlet pressure	500 Pa/113,000–260,000 Pa
Difference pressure	112.5 Pa/3000–150,000 Pa
Temperature/Thermocouple	0.1 K/313–377 K
Temperature/IR-Camera	0.3 K/313–413 K
Mass flow	0.1%/0.00019–0.0019 kg/s
Voltage	0.01 V/1.25–7 V
Electrical current	1 A/50–300 A

DC power supplies are connected in parallel to provide the necessary heat flux. Temperatures are measured at both inlet and outlet of the channel. Inlet pressure and pressure drop are also registered. After leaving the test section, the fluid condenses and returns to the reservoir. The experimental setup is open to the atmosphere after the condenser.

Once both mass and heat fluxes are set and after the desired operating conditions are reached, the temperature distribution of the channel is recorded by the IR-Camera. The data recording is performed by a ThermaCam® SC3000, manufactured by FLIR Systems. A high emissivity of the scanned surface is required to reduce the uncertainty of the IR temperature measurement. Therefore, the channel is coated with a very thin black lacquer, which provides an emissivity of approximately 0.95. The emissivity is a strong function of the structure and temperature of the surface, and, since the knowledge of the emissivity of the surface is essential to obtain reliable results, an intensive calibration is necessary to describe these dependencies and correct the measured temperatures. Two different calibration tests were carried out. First, the empty channel was electrically heated, and the wall temperatures were thermographically registered and compared with those read by thermocouples, which were positioned at different axial locations. These thermocouples measured the temperature inside the empty channel, which can be used to determine the temperature on the metallic surface of the channel, i.e. under the lacquer. The wall temperatures obtained in this way were compared with the temperatures read by the camera at the same positions. Second, preheated water flowing at high velocity was employed in order to check the calibration curves. The outer wall temperatures on the metallic surface were derived from the measured inlet and outlet temperatures of water. Thus, the outer wall temperatures measured by the camera were calibrated against the wall temperature of the metallic surface. Through these means, inhomogeneities of the lacquer layer can be detected and their influence on the experimental heat transfer coefficient can be eliminated.

The experimental accuracy of the measured values within the operating range is shown in Table 1.

3. Data reduction

As mentioned above, the temperature distribution of the wall is recorded at a frequency of 150 Hz for 25 s. The first

step in the data reduction is to determine the temperature profile to be used in calculating the heat transfer coefficients. Since significant oscillations of the temperature are observed, the recorded values are analyzed for each test fluid to determine the minimum period of time over which the average wall temperatures remain constant. These time averaged temperatures are used to calculate the inner wall temperatures in the procedure of obtaining the heat transfer coefficient.

The methodology of the data acquisition is presented in Fig. 2. An analysis area is positioned on each thermographic picture of the channel, so that the spatio-temporal temperature distribution on the channel surface is available for the data reduction. In this study, only the axial dependence of the temperature is considered. Thus, the temperature for each axial position is set to be the average of the temperatures corresponding to each pixel in a central region of the surface of the channel, approximately 3 mm wide, where the influence of the radial heat conduction can be neglected. The entire channel can be registered instantaneously with a spatial resolution in the axial direction of 0.7 mm/pixel.

The heat transfer coefficient is calculated according to Eq. (1):

$$\alpha = \frac{q}{(T_{\mathrm{iw}} - \overline{T}_{\mathrm{Fl}})} \tag{1}$$

The local heat flux, q, is calculated from the applied electrical power and accounting for the heat losses to the environment through natural convection and radiation. These heat losses are obtained from calibration tests, since they depend on the temperature of the outer wall and, therefore, also on the axial position. They represent between a 0.5% and 2% of the total input power. Both voltage and current are measured, but, since calibration tests are carried out for the electrical resistance of the channel, only one of them, viz. voltage, was used for the data reduction.

The fluid temperature is computed from an energy balance between the inlet and the corresponding axial position in the single-phase flow region, Eq. (2). For two-phase flow, the fluid temperature is set to be the saturation temperature at the measured pressure, Eq. (3). Only the axial dependence of the pressure is considered.

$$\overline{T}_{\mathrm{Fl}} = T_{\mathrm{Fl,IN}} + \frac{2q(h+w)}{mc_{\mathrm{Fl}}hw} z \quad \text{Single-phase region} \tag{2}$$

$$\overline{T}_{\mathrm{Fl}} = T_{\mathrm{B}}(p) \quad \text{Two-phase region} \tag{3}$$

As far as the pressure is concerned, single-phase measurements are carried out to determine the friction factor for all liquid phase. These coefficients are compared with the well-known prediction in Kakaç et al. (1987) for rectangular channels, and a good agreement is found. The pressure at the axial position where boiling begins is calculated from the measured inlet pressure and the calculated single-phase pressure drop. From there and for the two-phase flow region, the pressure drop is determined from the difference pressure measurement and accounting for the pressure drop corresponding to the single-phase region. The comparison of the measured pressure drops with some correlations available in the literature, like for example (Lee and Mudawar, 2005 and Lockhart and Martinelli, 1949), shows partly strong discrepancies not only between experimental and theoretical results, but also among the correlation values. Therefore, a linear pressure drop is assumed from the onset of boiling and during the two-phase flow region.

The inner wall temperature is calculated from the measured values of the outer wall temperature using the one dimensional steady state heat conduction equation with heat generation. The influence of the axial heat conduction was already discussed in Hapke et al. (2002) and found to be negligible under the here given conditions. The vapor quality is computed from an energy balance between the inlet and the corresponding axial position. The data reduction can be found in detail in Hapke et al. (2002).

The analysis of experimental uncertainties leads to an average error in the heat transfer coefficient of 15%.

Mass fluxes from 50 to 500 kg/m^{2}s and heat fluxes up to 400 kW/m^2 at an outlet pressure of 0.1 MPa are examined.

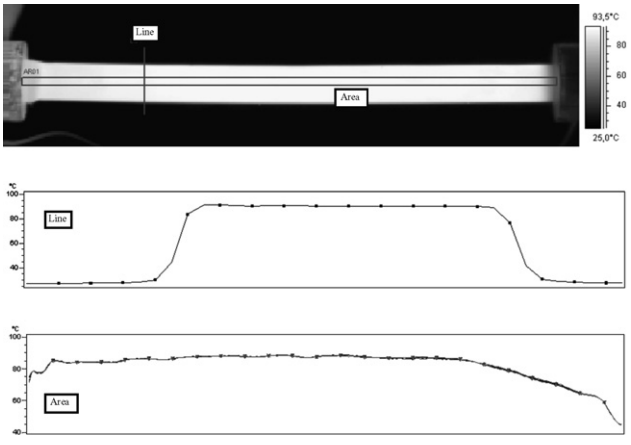

Fig. 2. Infrared image with analysis area and line and temperature profiles in the transverse (line) and axial (5 lines in the area) direction respectively.

4. Experimental results

4.1. Dynamic analysis

The registered outer wall temperatures over the measuring time for some axial positions are shown in Figs. 3 and 4 for water and ethanol respectively. Oscillations of the temperature can be clearly recognized. The amplitude and frequency of the oscillations vary depending on the operating parameters and also on the vapor quality. The oscillations are found to increase with increasing heat flux and with decreasing mass flux. Therefore, low mass fluxes and the corresponding maximum heat flux are selected for both water and ethanol. Fig. 3 shows the obtained temperature behavior for water. Low frequency oscillations can be

observed for low qualities. The maximum amplitude is found in the region of subcooled boiling, just before nucleate boiling begins. The maximum temperature difference in this region is found to be 30 K. The amplitude decreases strongly thereafter with increasing vapor quality. After the initial region, where nucleate boiling dominates, nearly constant wall temperatures are registered. A characteristic oscillation frequency of the wall temperature is not observed.

A completely different situation is observed for ethanol, Fig. 4. The amplitude remains approximately constant and its maximum value is lower than 5 K. The frequency of the temperature oscillations increases slightly with increasing vapor quality. Nearly periodic oscillations (frequency of approximately 5 Hz) are observed at higher values of vapor quality.

The oscillations of the wall temperature shown in Figs. 3 and 4 can yield different values and trends of the heat transfer coefficient. This transient behavior suggests that, in order to obtain reliable results, the temperature used for the calculation of the heat transfer coefficient should be time averaged. Therefore, the registered wall temperatures are averaged over increasing time periods to find out the minimum measurement time required to obtain constant values of the temperature. The time averaged wall temperatures are shown in Figs. 5 and 6 for both test fluids.

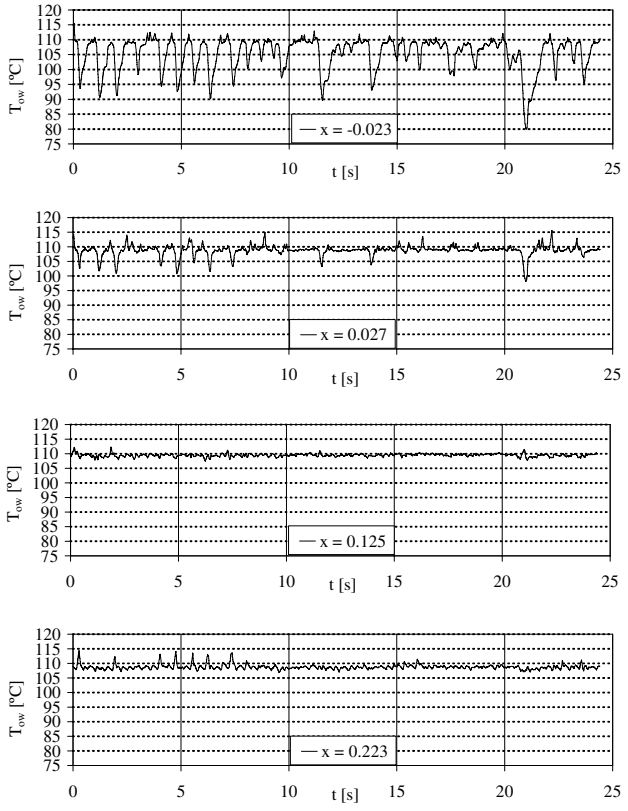

Fig. 3. Outer wall temperature over time for different values of vapor quality (i.e. different axial positions), water, $m = 100\ \mathrm{kg/m^2\ s}$, $q = 80\ \mathrm{kW/m^2}$.

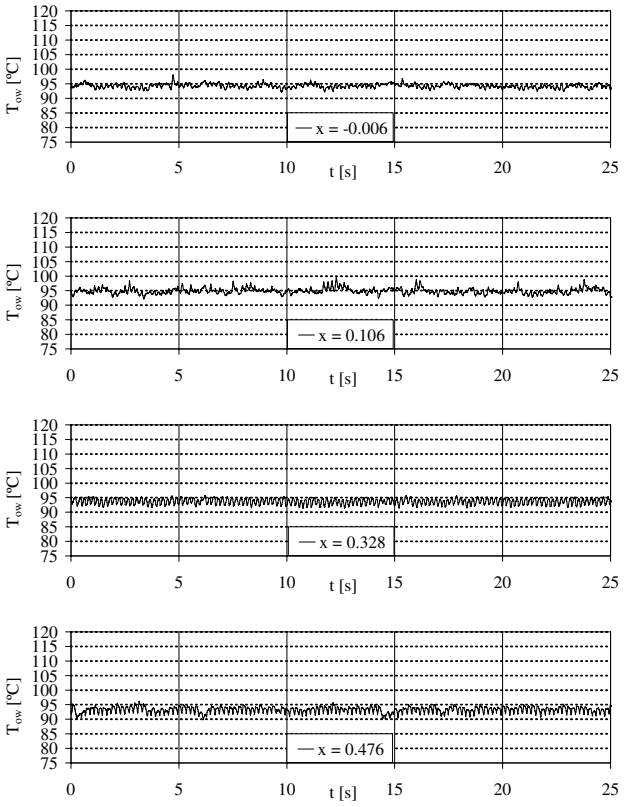

Fig. 4. Outer wall temperature over time for different values of vapor quality (i.e. different axial positions), ethanol, $m = 200\ \mathrm{kg/m^2\ s}$, $q = 90\ \mathrm{kW/m^2}$.

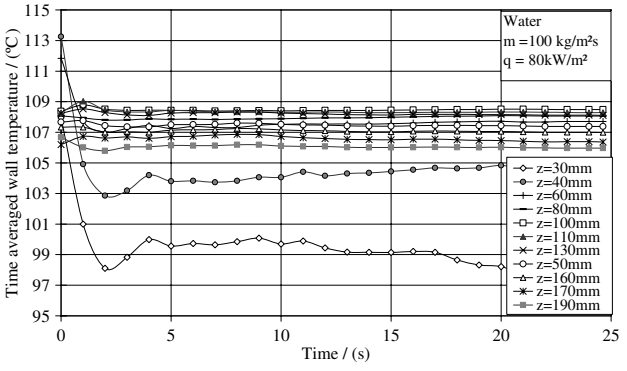

Fig. 5. Wall temperature versus averaging time interval, water.

In the case of water, the wall temperatures remain constant after approximately 5 s, especially for higher values of quality. As already seen in Fig. 3, pronounced instability of the wall temperature is found at low vapor qualities. Since the oscillation amplitude in the case of ethanol is smaller, the wall temperature remains nearly constant when averaged over only 3 s.

The oscillations of the temperature presented in this work are measured at the outer surface of the channel and an influence of the wall thickness, in this case 0.3 mm, on both attenuation of the amplitude and phase

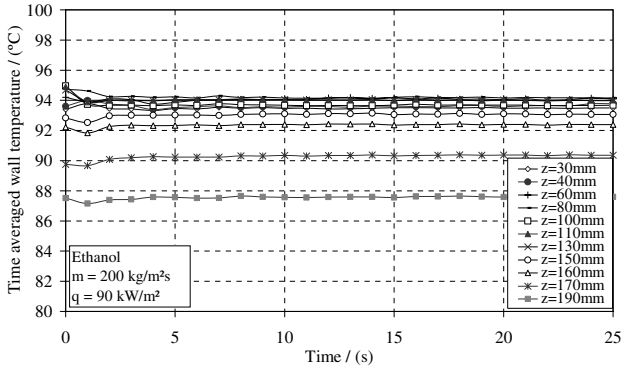

Fig. 6. Wall temperature versus averaging time interval, ethanol.

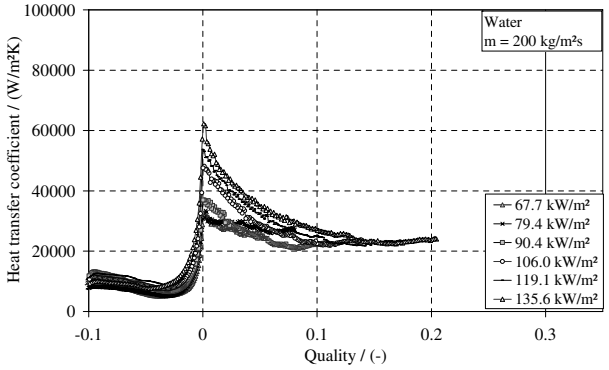

Fig. 8. Heat transfer coefficient over quality, water, $m = 200$ kg/m^2 s.

shift is expected. The effect of the heat conduction through the wall is analyzed by using the computer software FLUENT®. Initial results are shown in Fig. 7. In this case the wall temperature shown in Fig. 4 for a vapor quality of 0.328 is obtained by approximating the inner wall temperature by a sinusoidal function. Since the heat losses to the environment are low when compared with the heat generation, the outer wall is set to be adiabatic. One-dimensional heat conduction with heat generation is considered and periodic boundary conditions are set in the axial direction. Both inner and outer wall temperatures are shown in Fig. 7. It can be observed that, in this case, the wall thickness has a negligible influence on the phase shift. On the other hand, an attenuation of the amplitude of approximately 6% is found.

4.2. Heat transfer coefficients

The heat transfer coefficients are calculated for both test fluids using Eq. (1). The time averaged wall temperature is employed in each case to determine the inner wall temperature.

Figs. 8–10 show the calculated heat transfer coefficients over vapor quality for water at different heat fluxes and mass fluxes of 200, 400 and 500 kg/m^2 s. It can be observed that the heat transfer coefficient for water decreases with increasing quality and depends on heat flux. This behavior

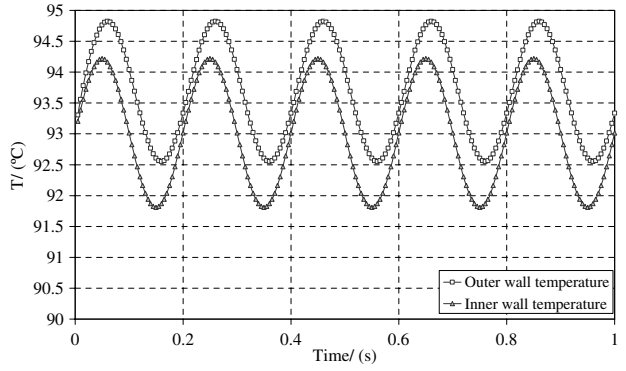

Fig. 7. Simulation results: outer and inner wall temperatures, ethanol, $m = 200$ kg/m^2 s, $q = 90$ kW/m^2, $x = 0.328$, Fo ($t = 1$ s) = 44.

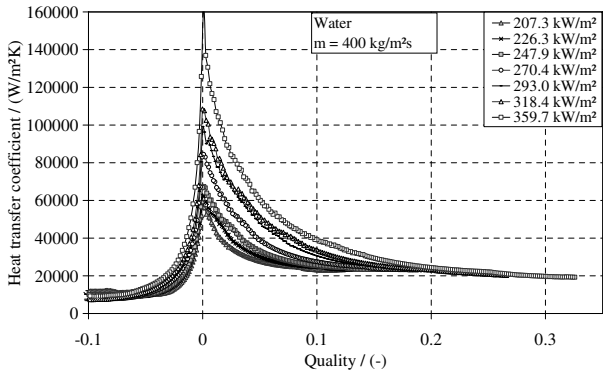

Fig. 9. Heat transfer coefficient versus quality, water, $m = 400$ kg/m^2 s.

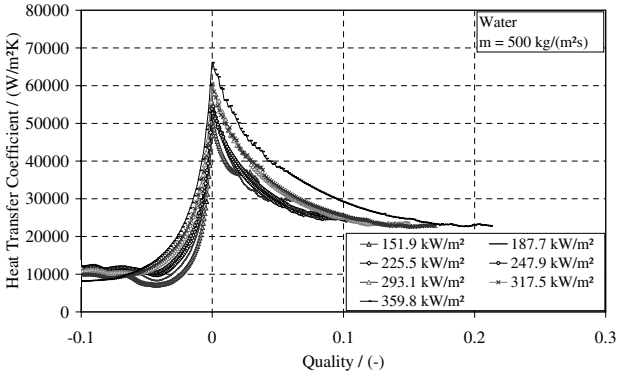

Fig. 10. Heat transfer coefficient versus quality, water, $m = 500$ kg/m^2 s.

has been already reported, for example in Kandlikar and Balasubramanian (2004). The decrease in the heat transfer coefficient for water can be explained by the special boiling behavior in small channels. Due to the space constraints, the vapor bubbles can reach a diameter which can be of the same order of magnitude as the channel size. This phenomenon leads to the occurrence of mechanisms such as bubbly flow, confined bubble, slug or plug flow and annular flow. According to (Kandlikar and Balasubramanian, 2004), the presence of nucleating bubbles at the walls and in the thin liquid film during slug and annular flow is

responsible for this decrease, which indicates the dominance of nucleate boiling. This explanation is consistent with some visualization reported in literature, (Kandlikar and Balasubramanian, 2004; Brutin et al., 2003). The experimental trend for water in this study differs from that reported in previous investigations by the authors, (Cortina Díaz et al., 2004), where convective boiling dominated. On the one hand, this discrepancy can be due to the use of different channel geometries and dimensions and to the different operating parameters. On the other hand, the heat transfer coefficients are measured here only within the low quality region. It is also possible that convective boiling could appear if higher qualities would have been considered.

In the case of ethanol, Figs. 11–13, the experimental trends of the heat transfer coefficient indicate that the heat transfer is also influenced by convective boiling. The heat transfer coefficient increases in the region of subcooled boiling and decreases immediately after the quality reaches zero. The heat transfer coefficients in this region depend on the applied heat flux. Thereafter, two different trends can be recognized in the two-phase region. At higher qualities and low heat fluxes, the heat transfer coefficient increases with increasing quality and is independent of the applied heat flux. For higher heat fluxes, the heat transfer coefficient decreases with quality. This change in the boiling behavior was already reported in Xu et al. (2005) and Lin et al. (2001).

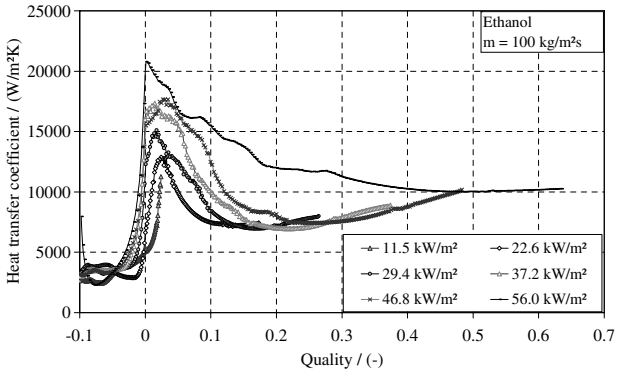

Fig. 11. Heat transfer coefficient versus quality, ethanol, $m = 100$ kg/m^2 s.

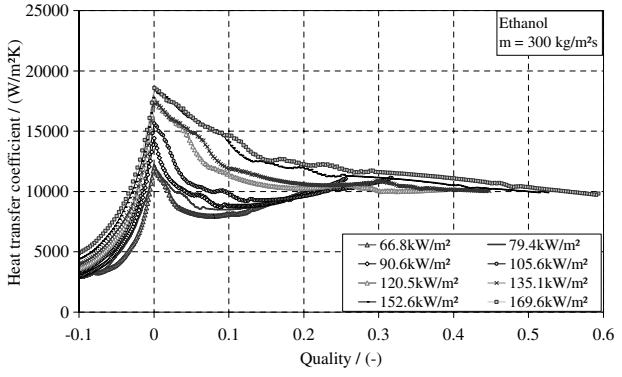

Fig. 12. Heat transfer coefficient versus quality, ethanol, $m = 300$ kg/m^2 s.

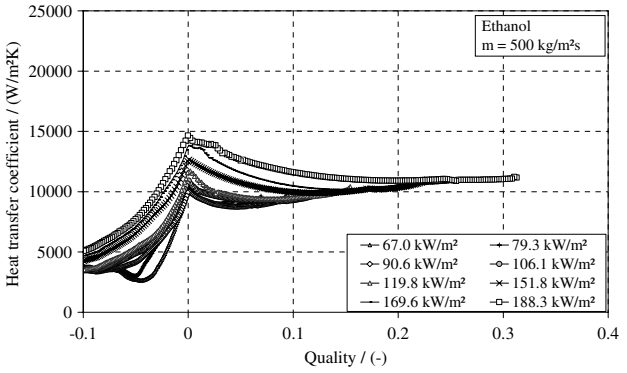

Fig. 13. Heat transfer coefficient versus quality, ethanol, $m = 500$ kg/m^2 s.

The experimental data are compared with the predictions of six widely used two-phase flow heat transfer coefficient correlations, viz. Kandlikar and Balasubramanian (2003), Liu and Winterton (1991), Lazarek and Black (1982), Steiner and Taborek (1992), Chen (1966), and Zhang et al. (2004). The Zhang et al. correlation is a modification of the Chen correlation. In the case of the Kandlikar correlation, only the nucleate boiling contribution to the heat transfer coefficient is considered for the present comparison. Figs. 14 and 15 show the experimental and

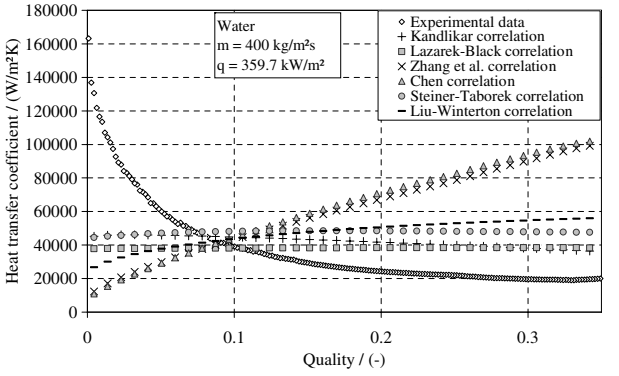

Fig. 14. Comparison between experimental and predicted heat transfer coefficients, water.

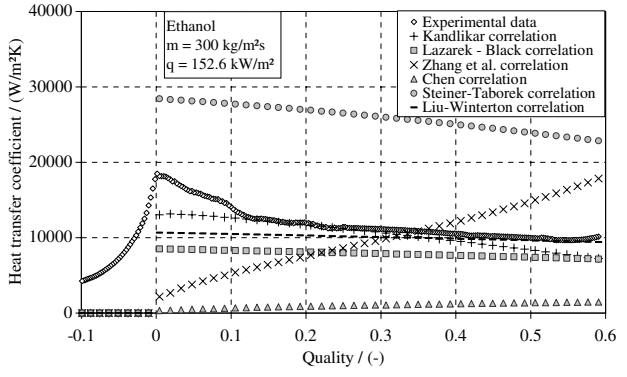

Fig. 15. Comparison between experimental and predicted heat transfer coefficients, ethanol.

predicted heat transfer coefficients for both test fluids and selected mass and heat fluxes.

The experimental trend of the heat transfer coefficient for ethanol is in relatively good agreement with the predictions of the Kandlikar and Liu-Winterton correlation. In the case of water, the experimental values are overpredicted by all the correlations. An increasing trend is predicted in nearly all cases, with exception of Kandlikar and Lazarek-Black correlations. Further research is needed to find out the reason for this discrepancy.

5. Conclusions

In the present study, infrared thermography was employed to obtain the wall temperature distribution. Images of the test section were recorded at a frequency of 150 Hz. Flow instability of boiling in microchannels, which has been often reported in the literature, was studied on the basis of oscillations of the wall temperature. High amplitude oscillations were found for water in the region of subcooled boiling at qualities slightly below zero. However, the amplitude decreased as quality increased and no characteristic frequency was observed. Flow boiling of ethanol yielded low amplitude oscillations of the wall temperature, even within the subcooled boiling region. Increase in quality resulted in increasing oscillation amplitude. Regular oscillations were measured for high values of quality. In order to obtain reliable values of the heat transfer coefficient, the outer wall temperatures were averaged over time.

The heat transfer coefficient was found to decrease with increasing quality for water. This trend is consistent with some studies in literature and indicates that nucleate boiling dominated in the low quality region.

On the other hand, different trends could be observed for ethanol after the low quality region. The heat transfer coefficient increased with increasing quality at low heat fluxes. With increasing heat flux, the heat transfer coefficient decreased with quality.

The experimental values were compared with those predicted by the correlations available in the literature. A qualitatively good agreement is found only for ethanol. The experimental values for water were generally overpredicted.

References

Bao, Z.Y., Fletcher, D.F., Haynes, B.S., 2000. Flow boiling heat transfer of Freon R11 and HCFC123 in narrow passages. International Journal of Heat and Mass Transfer 43, 3347–3358.

Brutin, D., Topin, F., Tadrist, L., 2003. Experimental study of unsteady convective boiling in heated minichannels. International Journal of Heat and Mass Transfer 46, 2957–2965.

Chen, J.C., 1966. A Correlation for Boiling Heat Transfer to Saturated Fluids in Convective Flow. Ind. Eng. Chem. Proc. DD. 5, 322–329.

Cortina Díaz, M., Boye, H., Hapke, I., Schmidt, J., Staate, Y., Zhekov, Z., 2004. Flow boiling in mini and microchannels. In: Proceedings of Second International Conference on Microchannels and Minichannels, Rochester, NY, USA, pp. 445–452.

Groll, M., Mertz, R., Minichannel heat transfer: an overview on activities in Europe. In: Proceedings of First International Conference on Microchannels and Minichannels, Rochester, NY, USA, 2003.

Hapke, I., Boye, H., Schmidt, J., 2002. Flow boiling of water and *N*-Heptane in microchannels. Microscale Thermophysical Engineering, 99–115.

Kakaç, S., Shah, R.K., Aung, W., 1987. Handbook of Single-Phase Convective Heat Transfer. Wiley-Interscience, USA.

Kandlikar, S.G., 2002. Fundamental issues related to flow boiling in minichannels and microchannels. Experimental Thermal and Fluid Science 26, 389–407.

Kandlikar, S.G., 2004. Heat transfer mechanisms during flow boiling in microchannels. Journal of Heat Transfer 126, 8–16.

Kandlikar, S.G., Balasubramanian, P. 2004. Effect of gravitational orientation on flow boiling of water in 1054×197 parallel minichannels. In: Proceedings of Second International Conference on Microchannels and Minichannels, Rochester, NY, USA, pp. 539–550.

Kandlikar, S.G., Balasubramanian, P. 2003. Extending the applicability of the flow boiling correlation to low Reynolds number flows in microchannels. In: Proceedings of First International Conference on Microchannels and Minichannels, Rochester, NY, USA.

Lazarek, G.M., Black, S.H., 1982. Evaporative heat transfer, pressure drop and critical heat flux in a small vertical tube. International Journal of Heat and Mass Transfer 25 (7), 945–960.

Lee, J., Mudawar, I., 2005. Two-phase flow in high-heat-flux microchannel heat sink for refrigeration cooling applications: Part I—pressure drop characteristics. International Journal of Heat Mass Transfer 48, 928–940.

Lin, S., Kew, P.A., Cornwell, K., 2001. Two-phase heat transfer to a refrigerant in a 1 mm diameter tube. International Journal of Refrigeration 24, 51–56.

Liu, Z., Winterton, R.H., 1991. A general correlation for saturated and subcooled flow boiling in tubes and annuli, based on a nucleate pool boiling equation. International Journal of Heat and Mass Transfer 34, 2759–2766.

Lockhart, R.W., Martinelli, R.C., 1949. Proposed correlation data for isothermal two-phase two-component flow in pipes. Chemical Engineering Progress 45, 38–48.

Shuai, J., Kulenovic, R., Groll, M., Mertz, R., 2004. Flow observation and flow pattern ttransition during flow boiling in narrow rectangular vertical channels. In: Proceedings of 6th International Symposium on Heat and Mass Transfer, Beijing, China.

Steiner, D., Taborek, J., 1992. Flow boiling heat transfer in vertical tubes correlated by an asymptotic model. Heat Transfer Engineering 13 (2), 43–69.

Thome, J.R., 2004. Boiling in microchannels: a review of experiment and theory. International Journal of Heat and Fluid Flow 25, 128–139.

Xu, J., Shen, S., Gan, Y., Li, Y., Zhang, W., Su, Q., 2005. Transient flow pattern based microscale boiling heat transfer mechanisms. Journal of Micromechanics and Microengineering 15, 1344–1361.

Zhang, W., Hibiki, T., Mishima, K., 2004. Correlation for boiling heat transfer in mini-channels. International Journal of Heat and Mass Transfer 47, 5749–5763.